

See discussions, stats, and author profiles for this publication at: <https://www.researchgate.net/publication/279862979>

Structural Changes in Ceramide Bilayers Rationalize Increased Permeation through Stratum Corneum Models with Shorter Acyl Tails

ARTICLE in THE JOURNAL OF PHYSICAL CHEMISTRY B · JULY 2015

Impact Factor: 3.3 · DOI: 10.1021/acs.jpcb.5b05522 · Source: PubMed

CITATIONS

2

READS

76

6 AUTHORS, INCLUDING:



Katerina Vávrová

Charles University in Prague

73 PUBLICATIONS 896 CITATIONS

[SEE PROFILE](#)



Russell Devane

Procter & Gamble

50 PUBLICATIONS 1,280 CITATIONS

[SEE PROFILE](#)



Michal Otyepka

Palacký University of Olomouc

181 PUBLICATIONS 4,541 CITATIONS

[SEE PROFILE](#)



Karel Berka

Palacký University of Olomouc

49 PUBLICATIONS 665 CITATIONS

[SEE PROFILE](#)

Structural Changes in Ceramide Bilayers Rationalize Increased Permeation through Stratum Corneum Models with Shorter Acyl Tails

Markéta Palonciová,[†] Kateřina Vávrová,[‡] Žofie Sovová,[†] Russell DeVane,[§] Michal Otyepka,[†] and Karel Berka^{*,†}

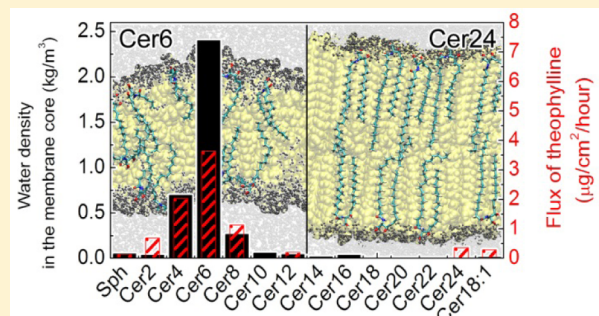
[†]Regional Centre of Advanced Technologies and Materials, Department of Physical Chemistry, Faculty of Science, Palacký University Olomouc, tř. 17. listopadu 12, 771 46 Olomouc, Czech Republic

[‡]Skin Barrier Research Group, Faculty of Pharmacy in Hradec Králové, Charles University in Prague, Heyrovského 1203, 500 05 Hradec Králové, Czech Republic

[§]Corporate Modeling & Simulation, Procter & Gamble, 8611 Beckett Road, West Chester, Ohio 45069, United States

Supporting Information

ABSTRACT: Ceramides are indispensable constituents of the stratum corneum (SC), the uppermost impermeable layer of human skin. Ceramides with shorter (four- to eight-carbon acyl chains) fatty acid chains increase skin and model membrane permeability, while further shortening of the chain leads to increased resistance to penetration almost as good as that of ceramides from healthy skin (24 carbons long on average). Here we address the extent to which the atomistic CHARMM36 and coarse-grain MARTINI molecular dynamics (MD) simulations reflect the skin permeability data. As a result, we observed the same bell-shaped permeability trend for water that was observed in the skin and multilayer membrane experiments for model compounds. We showed that the enhanced permeability of the short ceramides is mainly caused by the disturbance of their headgroup conformation because of their inability to accommodate the shorter lipid acyl chain into a typical hairpin conformation, which further led to their destabilization and phase separation. As MD simulations described well delicate structural features of SC membranes, they seem to be suitable for further studies of the SC superstructure, including the development of skin penetration enhancers for transdermal drug delivery and skin toxicity risk assessment studies.



INTRODUCTION

Ceramides (Cer) are key constituents of the skin barrier protecting our bodies against water loss and the entrance of undesirable chemicals from our environment.¹ As such, skin and especially its uppermost layer, stratum corneum (SC), are vital for maintaining stable conditions in the human body. Cer are sphingolipids, which in skin usually contain long saturated tails. Unlike phosphatidylglycerols, typical for cell membranes,² the Cer headgroup is rather small and serine-based, forming a network of hydrogen bonds.^{3,4} Also, pure Cer in aqueous solution does not form fluid bilayers but rather V-shaped gel phase lipid membranes of Cer or even lipid crystals,^{5,6} or spongelike structures that are dependent on the level of hydration and temperature.⁷ SC lipid mixtures also contain almost equimolar amounts of free fatty acid (FFA) and cholesterol (Chol) and other minor constituents.³ These lipids form highly ordered and weakly permeable membranes.⁸ This unusual membrane composition with a high Cer content is essential for maintaining the skin barrier function.⁹

The permeability of SC lipid membranes depends strongly on the Cer composition of these membranes.¹⁰ An increased

fraction of Cer with shorter fatty acid chains [with approximately 16 carbons (16C)] and a decreased amount of Cer with a typical fatty acid chain of around 24C (long Cer) is one of the signs of several skin diseases [apart from variations in Cer subclasses (for a review, see ref 11)], such as atopic dermatitis, psoriasis, or ichthyoses,^{12–16} and leads to an increased water loss and a reduced level of protection from allergens, pollution, and other xenobiotics. The permeability properties of the skin can be mimicked by model lipid membranes.¹⁷ In a recent study that aimed to elucidate the role of Cer chain length, it was shown that short Cer (4–8C) alone significantly increases skin permeability with maxima at 4–6C acyl.¹⁸ Such substantial changes in Cer acyl chain length are not encountered in diseased skin; however, understanding the chain length-dependent permeability would be interesting, in particular because Cer with 6C acyl are frequently used as easier-to-handle Cer mimics. However, both theoretical and

Received: June 9, 2015

Revised: July 7, 2015

experimental studies of the mechanism of such increased skin permeability seem to be complicated by the complexity of the skin composition and structure.

To reveal the effect of Cer acyl chain length on the SC lipid barrier, Školová et al.¹⁹ prepared model membranes consisting of equimolar mixtures of CerNS (*N*-lignoceroylsphingosine) or its shorter analogue, lignoceric acid (most abundant FFA in SC), and Chol with addition of a small amount of cholesterol sulfate. The lipid mixtures arranged themselves into multilayer membranes with a nontrivial bell-shaped permeability trend with the highest values for short Cer containing fatty acid chains with around 4–8C that was similar to the trend found in SC.¹⁸ Because the trend was reproduced well in the SC model multilayer membranes experimentally,¹⁹ it would be valuable to gain insight into this phenomenon by modern molecular dynamics (MD) simulations on a simple bilayer model.

MD simulations allow studies of complex systems simultaneously at atomistic and subpicosecond resolution, which is not possible using any of the experimental techniques. Most of the initial MD studies^{20,21} on lipid membranes were performed on fluid phosphatidylcholine bilayers, representing cell membranes, but until now, only a limited number of studies have focused on peculiarities of the simulations of gel phase membranes similar to the SC membrane.^{8,22} As the structure of the SC membrane is still not entirely known, most recent simulation studies focused on the structural properties of bilayers containing one or more SC components, e.g., Cer,^{5,23–26} while only recently were the first attempts to analyze SC multilayer superstructure performed.^{27,28} One of the main struggles in gel phase membranes is its rigidity, which increases the computational costs of such simulations. As the analysis of the penetration through the membrane requires even greater computational resources,^{29,30} it is not surprising that there are just a handful of MD simulations trying to analyze the penetration through the Cer-containing gel phase membrane.^{8,31–33} Although the representation of the SC multilayer membrane by a Cer SC-like bilayer is a crude simplification, the penetration through the artificially built gel phase bilayer alone was shown to impose a barrier for penetration much higher than that of a fluidic cell-like membrane.⁸ The major questions here are whether MD simulation would be capable of capturing the permeability trend and if a bilayer is a sufficient model for analyzing skin permeabilities of more complex lipid multilayers such as skin.

In this paper, we rationalized the bell-shaped relationship between Cer acyl chain length and the permeability of the SC lipid membranes at the atomistic and coarse-grain (CG) level using MD simulations. MD results depend heavily on a chosen force field (FF). The atomistic CHARMM36 FF for phosphatidylglycerols³⁴ was shown to reproduce well the available experimental properties.³⁵ However, this study is one of the first tests of the newly developed CHARMM36 FF for sphingolipids and Cer in particular.³⁶ Membranes are also being more frequently studied using a coarse-grain force field, such as MARTINI,³⁷ where typically a foursome of heavy atoms is replaced by so-called beads. This reduction of particles leads to a large acceleration of the simulations. As new MARTINI-compatible force field parameters for Cer were developed recently,⁷ we also decided to compare their ability to describe physicochemical properties of Cer bilayers with the results of atomistic simulations. Because experimental investigation of Cer mixtures showed phase separation to Cer-rich, FFA-rich, and Chol domains, we modeled not only the mixture

of the major components but also pure FFA and pure Cer bilayers. Finally, we monitored the structural parameters of the bilayers as well as the conformations of Cer that play a crucial role in the resulting permeability.

METHODS

We prepared bilayers of equimolar mixtures of ceramide NS [with appropriate chain lengths from the shortest Sph and Cer2 through short Cer with C4–C10 until long Cer with C12–C24 (see Figure 1)], lignoceric acid [free fatty acid (FFA)], and

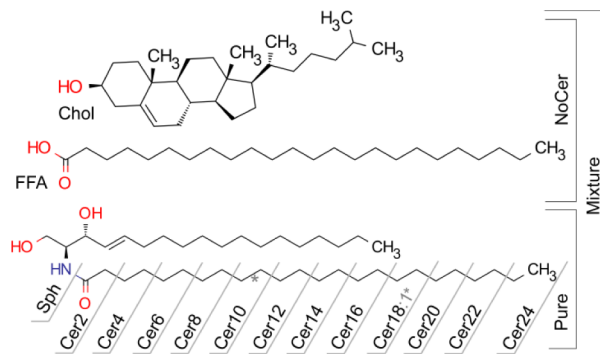


Figure 1. Molecular components of the lipid bilayers used in this study with abbreviations of the ceramide (Cer) analogues and free sphingosine (Sph). An asterisk denotes the position of the cis double bond in the Cer18:1 fatty acid tail.

cholesterol (Chol) and bilayers composed of a mixture of Chol and FFA (NoCer), which correspond to the experimental compositions of Školová et al.¹⁹ Though the experimental measurements were performed on either multilayers or monolayers of lipids, we studied their properties by lipid bilayer models. Also, a CG simulation suggested the formation of a spongelike phase⁷ instead of bilayers separated by water layers. However, this phenomenon cannot be seen in a small simulation box with a single bilayer hydrated with a thick layer of water. To better mimic experimentally observed conditions, as a phase separation of Cer-rich regions has been experimentally proposed,¹⁹ we prepared pure bilayers composed of only Cer and a bilayer composed of only FFA (FFA) to mimic Cer-rich and FFA-rich phases. In addition to focusing on the Cer studied experimentally,¹⁹ we also conducted simulations using other chain lengths in the series.

Topologies for ceramide NS (Cer) and Chol were derived from sphingomyelin parameters in the CHARMM36^{34,36,38} format and are presented in the Supporting Information. Topologies for Cer with shorter lipid chains were adjusted by removing the aliphatic middle atoms of the 24:0 chain. The topology of uncharged FFA was prepared by combining the acyl chain parameters from Cer and the acetic acid headgroup of the CHARMM General Force Field (cgenff).³⁹ All parameters were then transferred into GROMACS format and are presented in the Supporting Information.

Both mixed and pure bilayer structures were obtained using an in-house membrane builder. The pure bilayers contained 128 lipids arranged in a fully hydrated lipid bilayer with TIPSP water. The mixed membranes contained an equimolar mixture of 108 total lipid molecules equally distributed into a fully hydrated bilayer with at least 20 waters per lipid. The hydrated membranes were then equilibrated, and the remaining water was removed from the membrane core.

All atomistic MD simulations were performed using the GROMACS 5.0 simulation package.^{40,41} The simulations were performed under periodic boundary conditions in all directions with a 2 fs time step, using the Nosé–Hoover thermostat method^{42,43} and semi-isotropic pressure (1 bar) coupling using the Parrinello–Rahman barostat method.⁴⁴ As used also previously³⁵ for the CHARMM36 force field, van der Waals interactions were switched off to zero between 0.8 and 1.2 nm distances of interacting atoms and electrostatic interactions were treated by particle mesh Ewald from 1.2 nm.

For isothermal simulations, we performed 500 ns simulations at 310 K for both mixed and pure bilayers. After initial equilibration (50 ns), the systems reached stable properties, and we analyzed the macroscopic structural properties of the bilayers, such as area per lipid and membrane thickness (defined as the distance between the highest density of nitrogen atoms); we also monitored deuterium order parameters of acyl tails ($S_{(CD)}$, by standard GROMACS tool `g_order`). Further, we evaluated the water content in the middle of the pure Cer membranes and Cer headgroup organization.

As the lipid phase is directly related to the area per lipid (APL),⁴⁵ we evaluated the stability and phase transitions of the membranes based on the variation in area per lipid during heating. We let the bilayers equilibrate for 20 ns at 300 K and then heated them gradually to 400 K over the next 180 ns. We are aware of the high rate of heating (0.56 K/ns); therefore, we took into account only large and irreversible changes in the area per lipid versus temperature slope.

For coarse-grain (CG) simulations using the MARTINI-compatible force field,³⁷ we also prepared fully hydrated (at least 28 water beads per lipid; each water bead represents four water molecules) bilayers consisting of 512 Cer. These bilayers were constructed using the `insane.py` script (freely available at <http://md.chem.rug.nl/cgmartini>). For full length Cer, we used our recently introduced CG parameters,⁷ while for the short Cer, topologies were derived by shortening the C24 acyl tail. The acyl tail of oleoyl-Cer was mapped in the same manner as the sn-2 tail of POPC.³⁷ CG systems were denoted with the same system as in all atom simulation, CerNCG, where N stands for the number carbon atoms that would correspond to the number of carbons in an all atom representation. Thus, Cer4CG corresponds to (atomistic) Cer4 and has one CG bead, Cer24CG corresponds to Cer24 and has six CG beads, etc. All CG simulations were performed using the GROMACS 4.0.7 simulation package.⁴⁰ Systems were relaxed by 1000 steps using steepest descent geometry optimization followed by a series of short *NVT* and *NPT* MD simulations (1000 steps each) with increasing time steps of 1, 2, 5, and 10 fs. Finally, a 30 fs time step was used for production simulations (6 μ s for each system) at 310 K with separate velocity-rescaling thermostats⁴⁶ for Cer and water and Berendsen pressure coupling⁴⁷ (10^5 Pa) with the compressibility set to 4.6×10^{-10} Pa⁻¹. van der Waals interactions were shifted to zero between 0.9 and 1.2 nm, and Coulombic interactions were not considered. Pair lists were updated every 10 steps. Analyses of the last 5 μ s of simulations were performed using standard GROMACS tools. APL and membrane thickness were computed as described previously.⁴⁸ The order parameter S_{CC} was computed using the `do-order.py` script (freely available at <http://md.chem.rug.nl/cgmartini>). The conformations of Cer were determined on the basis of the angle between the terminal tail beads and the H1 headgroup bead (containing a nitrogen atom).

RESULTS

The Area per Lipid and Membrane Thickness Depend on Ceramide Chain Length. We analyzed the macroscopic structural parameters of Cer bilayers and observed an increase in the bilayer volume with an increasing Cer chain length (Figure 2). The chain length and area per lipid (APL) are

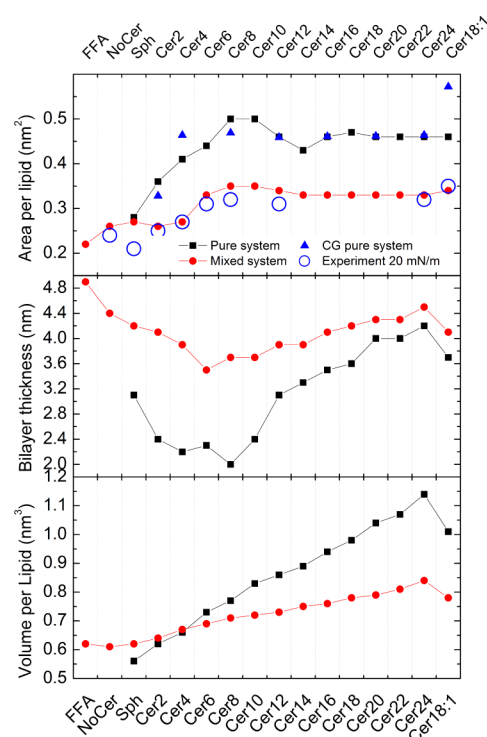


Figure 2. Area per lipid (top), bilayer thickness (middle), and volume per lipid (bottom) of pure (black line with squares) and mixed (red line with dots) Cer bilayers. The area per lipid is compared to the experimental area per lipid of the monolayer mixture at 20 mN/m from ref 19 (top, blue circles) and to CG pure systems (blue triangles). NoCer stands for a membrane composed of only FFA and Chol; FFA is composed of only FFA.

initially linearly correlated in pure bilayers; APL grows from Sph (0.28 nm^2) to Cer8 (0.50 nm^2 for both Cer8 and Cer10). However, further elongation does not lead to an additional APL increase (Cer12 and longer Cer all have similar APLs of $\sim 0.46 \text{ nm}^2$), but rather to an increase in membrane thickness for a pure bilayer (Figure 2). Pure bilayers have the smallest bilayer thickness at Cer8 (2.0 nm), whereas shortening or lengthening the chain leads to an increase in bilayer thickness. The APL from CG simulations nicely fits the atomistic simulation for pure bilayers with the exception of Cer18:1 (Figure S8 of the Supporting Information). In mixed bilayers, the thickness decreases from FFA (4.9 nm of the bilayer) to Cer6 (3.5 nm). From Cer6, the bilayer thickness grows with lipid chain length to Cer24 (4.5 nm). A double bond in Cer18:1 increases APL and decreases D_{HH} . APL values of Cer4–Cer8 show larger fluctuations (Figure S1 of the Supporting Information). In mixed bilayers, both APL and bilayer thickness are less dependent on the chain length than in the case of pure bilayers. Further, in mixed systems, the APL is almost constant above Cer6 ($\sim 0.33 \text{ nm}^2$).

The Lowest Level of Ordering Was Observed in Cer6 and Cer8 Membranes. We also analyzed average deuterium

order parameters [$S_{(CD)}$] (see the [Supporting Information](#) for the proper definition) of the lipid tails and observed lower $S_{(CD)}$ in bilayers with short Cer ([Figure 3](#)). Overall, the $S_{(CD)}$

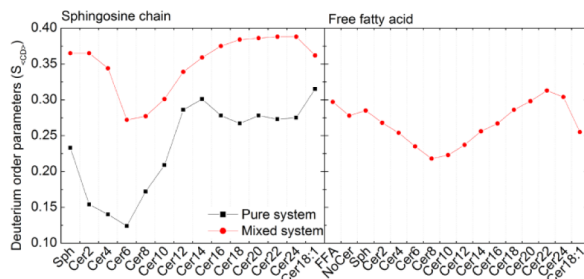


Figure 3. Average deuterium order parameters calculated for sphingosine chains of Cer (left) and FFA in the mixtures (right).

values of sphingosine chains were lower in pure bilayers than in the mixed bilayers, which was also affected by a smaller tilt angle in mixed bilayers ([Figure S2 of the Supporting Information](#)). In the case of pure lipid bilayers, we observed the lowest $S_{(CD)}$ for Cer2–Cer6 (~0.14) and in mixed bilayers for Cer6 and Cer8 (0.27). We analyzed the $S_{(CD)}$ for FFA in the mixed system, and here we observed the lowest $S_{(CD)}$ for Cer8 and Cer10 membranes [0.22 ([Figure 3](#) and [Figure S3 of the Supporting Information](#))]. The order parameters of the plateau region of FFA in the Cer24 mixture go to ~0.4, which agrees with experimental findings for stearic acid in a Cer mixture (~0.4).⁴⁹ The pure FFA bilayer was also significantly ordered, with ordering and tilt angles similar to those of the pure Cer24 bilayer (tilt angles of ~27° and ~24° for FFA and Cer24 bilayers, respectively). Increasing or decreasing the chain length below six or above eight carbons leads to an increase in the order parameters for both FFA and Cer24.

Ceramides Undergo a Phase Transition toward a Nonlamellar or Liquid-Disordered Phase. We monitored the temperature dependence of APL and evaluated the phase behavior based on the changes in APL while heating the simulation system. Experimentally, Cer24 exhibits two phase transitions, from an orthorhombic gel to a hexagonal gel phase at ~333 K and from a hexagonal gel phase to a disordered phase (liquid crystalline, LQ) at ~371 K.¹⁸ However, while the transition between the orthorhombic and hexagonal phases is visible in FTIR spectra as a disappearance of the splitting of

methylene scissoring or rocking band, the experimental APL measurement for that phase transition is almost unchanged,⁵⁰ and therefore, we focused on large changes in APL trends showing more visible transitions. The phase transition temperature between the gel and LQ can be visible during the evolution of APL during heating scans of simulated lipid bilayers, while it is impossible to read it from cooling scans of the same samples.⁵¹ In our simulations in pure Cer bilayers, long Cer [Cer24, Cer18:1, and Cer12 ([Figure 4](#))] show a steep enlargement of APL, indicating gel → LQ phase transitions. As the Cer tails become shorter, transition temperatures become lower, as well. Note also that in our case the system is heated throughout the simulation quite quickly (0.56 K/ns), resulting in a nonequilibrium simulation, unlike in the case of isothermal simulations. This leads to large APL fluctuations, and therefore, we can evaluate only permanent and sharp changes in the APL versus temperature scans and use them for approximate predictions of the phase transition temperature; however, we are unable to describe all possible transitions, e.g., orthorhombic → hexagonal gel phase transitions. Sph and short Cer [Cer6 and Cer8 ([Figure 4](#))] show rather complex behavior; the APL of rather disordered bilayer even at low temperatures is gradually growing with increased temperature with several steps and drops that cannot be significantly evaluated because of the nonequilibrium conditions. Above ~380–390 K, the bilayers lose their lamellar structure. This is, however, not the case for Cer2 and Cer4, which seem to be more stable than Cer6 and Cer8 (though Cer4 seems to be less stable than Cer2). In a manner consistent with the known ability of cholesterols to broaden the phase transition,⁵² we observed continuous growth of the APL with temperature for Cer mixtures with no irreversible transitions as observed for pure Cer ([Figure S4 of the Supporting Information](#)). In all, the most unstable systems were formed with pure Cer4, Cer6, Cer8, and Sph.

Water Penetrates inside Pure Ceramide Membranes.

During the free simulations, a significant amount of water molecules spontaneously penetrated into the pure short Cer bilayers but not in the mixed membranes. The water content of pure Cer bilayers increased with chain length from Sph to Cer6 and dropped again for Cer8 ([Figure 5](#)). Water molecules penetrated as funnel-like strings forming a semipore reaching the middle of the bilayer ([Figures 6 and 7](#)). Very few water molecules penetrated into long Cer bilayers. However, in the case of a water drop artificially formed in the middle of the membrane during the equilibration step, this drop stayed

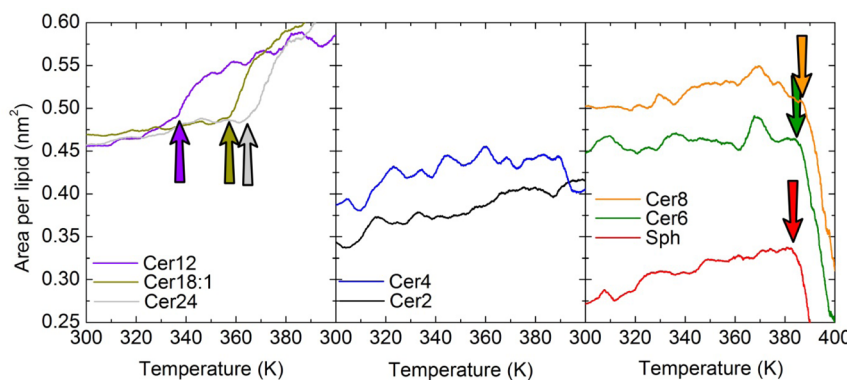


Figure 4. Dependence of area per lipid on temperature in pure Cer membranes (only experimentally studied lipids are shown for the sake of clarity). The steep increase in area per lipid in the left panel shows a gel–liquid crystalline transition. The strong decrease in the right panel in Sph, Cer6, and Cer8 shows a transition toward a nonlamellar phase.

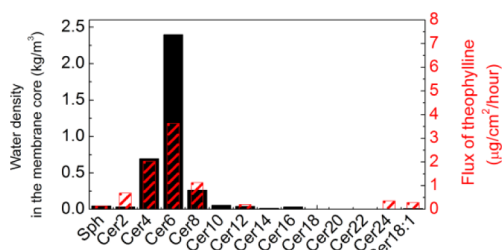


Figure 5. Water content in the middle of the membrane (black bars) compared to experimentally measured flux of theophylline (red bars) from ref 19.

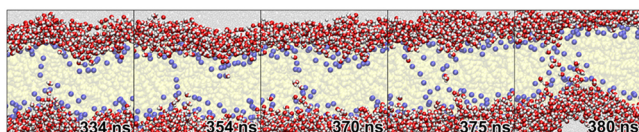


Figure 6. Snapshots of water penetrating into the membrane in a pure Cer6 bilayer. Cer6 is colored yellow. Nitrogen atoms are colored blue. Bulk water is shown as gray dots. Water molecules in contact with Cer are shown as white and red spheres.

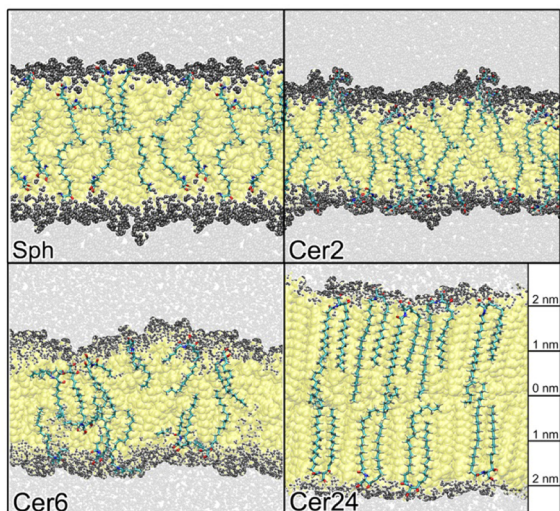


Figure 7. Snapshots of Sph, Cer2, Cer6, and Cer24 membranes. In Cer6, the water penetrating into the middle of the membrane is visible, while the Cer24 bilayer "stayed dry". The Cer6 membrane has significant undulation, while Sph and Cer2 are flatter. The gray dots represent water molecules; the yellow background displays the membrane, and some (not all) Cer molecules are shown as sticks.

trapped in the membrane of long Cer but was repelled when the membrane formed in short Cer (these data were not included in water content analysis). The density of water in the middle of pure Cer membranes corresponds closely to the permeability of these membranes to small hydrophilic molecules.

Longer Aliphatic Chains Interdigitate in the Membrane Core. At the atomistic level, we observed interdigitation of FFA or long Cer chains in the bilayer core (Figures 7 and 8). Pure Cer with shorter chains (from Sph until Cer10) formed disordered layers. The long lipids (from Cer12 up) formed highly ordered gel bilayers with significant chain interdigitation, resulting in a flexible disordered region in the bilayer center. The significant exception to the trends here is the FFA system; FFA molecules are not interdigitated and are highly ordered across the whole membrane region (Figure 8 and Figure S5 of the Supporting Information). In mixed bilayers, short Cer formed two ordered layers separated by a disordered region composed mostly of FFA tails in the membrane center. Cer chains are localized either in headgroups [shorter chain (see the next paragraph)] or in ordered layers (longer chains, sphingosine chain). Cholesterol is also located mostly in the ordered layers. The NoCer system is arranged in a similar way; both bilayer leaflets are organized and composed of FFA and Chol and are separated by a disordered region composed of interdigitated FFA chains. Elongation of Cer leads to incorporation of Cer chains into the middle FFA tail rich disordered layer, thus ordering it.

Shorter Ceramide Tails Are Oriented into the Head-group Region. A detailed analysis of the angles between terminal methyl carbons and nitrogen in headgroups showed significant conformational changes depending on the chain length. In well-ordered long Cer bilayers, the angle between the tail carbons is $\sim 17^\circ$ (Figures 8 and 9 and Table S1 of the Supporting Information). Decreasing the acyl chain length below 10 carbons leads to a significant increase in this angle, and the shorter acyl chains are then oriented into the headgroup area instead of being incorporated into the lamellar lipid structure. This is consistent in both pure and mixed Cer bilayers.

DISCUSSION

Pure Ceramide Bilayers Are More Sensitive to Acyl Chain Length Than Mixed Systems. In our model simulations of pure bilayer systems, long Cer are highly ordered while short Cer adopt a more disordered phase. When initially arranged into the bilayer, the most abundant Cer in the human SC (Cer24) forms an ordered bilayer with a dry interior, tilted lipid chains, and a sharp boundary between Cer

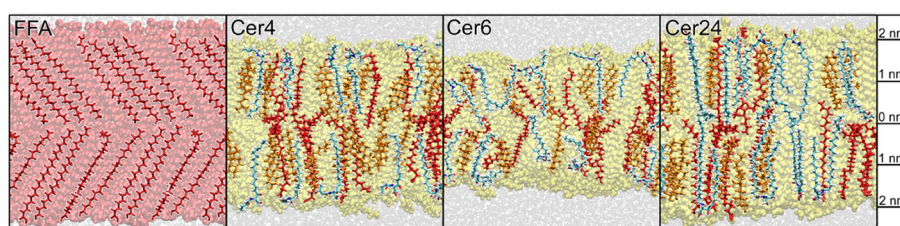


Figure 8. Membrane composed of pure FFA (left) and mixed membranes composed of Cer4, Cer6, and Cer24 (blue) with Chol (orange) and FFA (red). In Cer4, the middle of the membrane is formed almost entirely with FFA, and Cer chain elongation leads to an increasing level of interdigitation of Cer tails.

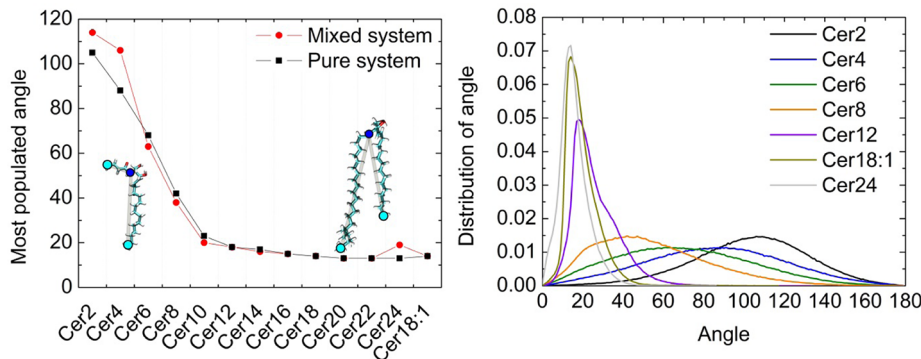


Figure 9. Most populated angles between terminal methyls of Cer chains and nitrogen (left) and angle distribution plots (right; only some of the Cer are shown) are very similar for both pure (displayed) and mixed membranes.

and water (Figure 7). In agreement with previous studies, the part of the bilayer occupied by both lipid tails is highly ordered,^{8,24} while the middle layer formed by interdigitated Cer acyl chains is disordered. Shortening of Cer acyl chain leads to more disordered membranes with significant undulation at 310 K and lower order parameters (Figure 3), affected by a significant tilt angle (Figure S2 of the Supporting Information). The decreased ordering was also experimentally observed on Cer6, Cer8, and Cer12 using FTIR spectra of pure Cer; the typical orthorhombic packing was not observed in those experiments.¹⁸ The disordered regions were also reported experimentally in Cer/FFA/Chol/CholS mixtures, where short Cer showed larger portions of disordered phase content probably located in phase-separated Cer-rich domains.¹⁹ Though the preference of short Cer for the disordered phase has been repeatedly reported,^{19,53} the phase transition temperature (T_m) experimentally measured for short Cer is interpreted as the gel → liquid crystalline phase transition. We suggest here the reconsideration of this interpretation, as the short Cer may be as well in the disordered or partially disordered phase at body temperature.

The adoption of the disordered phase is mainly caused by arrangement of a shorter lipid chain. When inspected in simulations, short Cer are not present in a hairpin orientation, but they are more likely arranged in an L shape or even an extended-like conformation (Figure 9 and Table S1 of the Supporting Information). The elongation of the acyl chain arranged in an L shape leads to an increase in the APL, while the hairpin-oriented Cer all possess similar APL values (Figure 2 and Figure S8 of the Supporting Information for the CG model). Though we did not observe long Cer arranged in an extended conformation, they might be arranged in this way in multilayers or crystals with slightly different structural properties, such as the lamellar repeat distance. When heated, long Cer go through a phase transition from the gel phase to the liquid crystalline phase, while the shorter ones collapse into a nonlamellar phase (Figure 4). Overall, pure Cer membranes are very sensitive to Cer chain length.

The addition of Chol and FFA stabilizes Cer bilayers and makes them less sensitive to the length of the Cer chain. The APL of mixed bilayers is lower than those of pure bilayers (Figure 2), with the only exception being Sph bilayers that possess the same APL as the NoCer mixture (FFA and Chol). On the other hand, bilayer thickness is larger in mixed bilayers than in pure ones. The development of APL during heating is more complex in mixed bilayers (Figure S4 of the Supporting Information); however, no nonlamellar transition was observed

for any of the systems. The behavior of Cer mixtures is in agreement with former studies of cholesterol and phosphatidylcholines, where increases in order parameters and broadening of the phase transition were also observed.⁵⁴ However, increasing the $S_{(CD)}$ and bilayer thickness is here mostly caused by a reduction in the tilt angle of Cer in mixed system (Figure S2 of the Supporting Information) and not by ordering of the bilayer, though visually, the pure bilayers are more ordered (Figures 7 and 8). The NoCer system also formed an ordered bilayer (Figure 3), but in the simulations of mixtures, FFA arranged into ordered leaflets and their tails formed a disordered mobile region in the bilayer core. This is in contrast with FTIR spectra that show a high degree of order for FFA even in the most permeable membranes¹⁹ and supports the experimental observation of phase separation. The FTIR spectra are in agreement with the FFA bilayer that formed a highly ordered, tilted layer (Figure 8 and Figure S5 of the Supporting Information). Because of time and size limitations, mixture simulations did not reproduce the phase separation experimentally expected. Consequently, from the atomistic simulation point of view, a mixed bilayer is not the best model for experimental Cer/FFA/Chol/CholS mixtures. Two independent models, including (1) impermeable FFA or NoCer bilayers and (2) a permeable pure Cer bilayer, better capture the experimental behavior.

The Incorporation of the Shorter Acyl Chain into the Headgroups Destabilizes Short Cer Bilayers. We observed that the permeability of small hydrophilic molecules through multilayers of Cer mixtures could be successfully modeled by a pure Cer bilayer. One would expect that the mixed lipid bilayer should reproduce theophylline/water penetration in mixed experimental systems, but no water penetrating into those bilayer models was observed. The phase separation, as was discussed in the previous section, suggests different interactions of molecules with various membrane phases. We monitored water molecules spontaneously penetrating into pure Cer bilayers and observed good correlation with the experimental flux of the small hydrophilic molecule theophylline (Figure 5). Small hydrophilic molecules permeate via free volume diffusion,⁵⁵ and we suggest that theophylline uses a mechanism similar to that of water; also, a mild correlation of the permeation of theophylline and TEWL was observed previously.⁵⁶ Moreover, theophylline permeation might be directly influenced by the presence of water in the membrane. The different permeability and quantity of water inside short Cer (Cer4–Cer6) membranes stem from a different structural organization.

The major contribution for the permeability of the membrane for hydrophilic molecules seems to be the conformation of lipids in the headgroup area driven by the length of the acyl tail. The significant conformational changes that we observed in this region result in a lower phase stability (Figure 4) and a higher permeability for water (Figure 5). While all long chain Cer molecules are in the hairpin conformation with a narrow peak in the terminal carbon angle distribution (Figure 9 and Table S1 of the Supporting Information), a decrease in the acyl chain length leads to broadening of the angle distribution and the acyl chain is oriented in the headgroup region (Figures 7–9). Similar behavior was previously observed in oxidized PC membranes, where it was linked with increased water permeability as well as enhancement of formation of water defects and pores.⁵⁷ Naturally, such a disturbance also influences the stability of the bilayer (Figure 4). We observed a nonlamellar transition for Sph, Cer6, and Cer8 and a drop in the APL in Cer4. The lower stability of these membranes also results in a lower energy barrier for their disturbance by a permeating substrate, which can be hypothesized as a local membrane phase transition event.

The permeability of lipophilic molecules is proposed to follow lateral diffusion in the membranes^{55,58} and is also affected by the mobility or ordering of membrane lipids. A correlation between the order parameters of lipid chains and permeability was found for phosphatidylcholine mixtures with cholesterol,⁴⁵ and we can assume a similar relationship in Cer: the higher the order parameters, the lower the permeability. The lowest order parameters were found for Cer6 and Cer8 in mixed systems and also for Cer6 in the pure system (Figure 3) and reflect well the most permeating systems.

MD Simulations with Used Force Field Parameters Reproduce Well Experimental Properties of Cer. We focused here on the ability of MD simulations to capture the trend of different permeabilities of Cer with varying tail lengths. The APL, trends in $S_{(CD)}$, or spontaneous water permeability reproduces well the experimentally observed properties (for more discussion of FF issues, see the Supporting Information). Though the only difference between the systems is the length of one acyl chain, the crucial differences appeared to be localized mainly in the headgroup conformation. The input parameters (FFs) of the headgroups were identical in all simulations in the respective force fields and appeared to be capable of modeling hairpin, L shape, and extended Cer conformations. As multiple experimentally derived SC models have been published and all of them have been based on a multilayer structure, this can be crucial for such modeling. For example, the Norlén⁵⁹ and Kiselev⁶⁰ models consider the extended conformation of Cer as a crucial connection between the SC layers. Moreover, the water spontaneously penetrating into pure Cer reflects very precisely the experimentally observed permeabilities of theophylline. From knowledge gained by comparison of experimentally observed permeabilities and simulated properties, we can assume that Cer10 (not studied by experiment) will still belong to more permeable Cer, while all other long Cer possess strong barrier properties. Together, MD simulations with MARTINI and CHARMM36 FF appeared to be very effective for SC superstructure and CHARMM36 FF also for the permeability studies.

CONCLUSION

In this paper, we rationalized in the atomistic resolution the increased permeability of model skin lipid membranes composed of short Cer. Though the experimental observations are performed on model mixture multilayers, we focused on the ability of the MD simulation to model their properties by simple bilayers. In our simulation models composed of either lipid mixtures or pure Cer arranged into bilayers, we observed that the shorter Cer chains do not incorporate into the lipid chain matrix of the bilayer but instead reside in the membrane headgroup region. Their shorter chains disrupt the close packing that is typical for the skin lipids. Consequently, they influence the area per lipid, lipid ordering, mobility of lipid atoms, phase stability of the bilayer, and bilayer permeability. The experimental evidence of the preference of shorter chain Cer for the disordered phase has been also observed,^{19,53} and here we present a similar theoretical proposal. Therefore, we suggest a reconsideration of this experimental interpretation as the shorter chain Cer (Sph-Cer10) may be present in a phase more disordered than previously thought as they have a weaker preference for hairpin conformation typical for Cer bilayers mimicking gel phase membranes. The crucial property of the disturbing chain appeared to be its length. Although the shortest Cer (Cer2) chains reside more in the headgroup region, they are not long enough to sufficiently disturb the membrane structure to allow increased permeability. With increasing lipid chain length, this disturbance grows until the hairpin conformation prevails. The short Cer (Cer4, Cer6, and Cer8) are then shown to be the most permeable in agreement with the experiment with addition of Cer10, which was not studied by experiment, while this effect was more pronounced in pure Cer membranes effectively modeling the effects of experimentally observed phase separation. We believe that knowledge of the relationship between lipid composition and arrangement and, consequently, the permeability of the skin lipid barrier will bring another perspective to our understanding of skin diseases such as atopic dermatitis, psoriasis, or ichthyoses. This knowledge should also extend to toxicological risk assessment and more rational development of barrier repair strategies. Finally, more mechanistic knowledge of permeation through the stratum corneum lipids would be beneficial in the field of transdermal/topical drug delivery, including permeation enhancing strategies.

ASSOCIATED CONTENT

Supporting Information

Area per lipid fluctuation during isothermal evolution (Figure S1), average tilt angles of sphingosine chains (Figure S2), individual deuterium order parameters and definition of order parameters (Figure S3), dependence of area per lipid on temperature in mixed Cer membranes (Figure S4), structure of the FFA and NoCer system (Figure S5), Cer headgroup organization (Table S1), a discussion concerning force field performance, structures of CG simulation systems (Figure S6), $S_{(CC)}$ order parameters in the CG simulation (Figure S7), structural parameters stemming from CG simulations (Figure S8), average B factors for the most fluctuating carbons and corresponding results (Figure S9), and topologies for Cer, FFA, and Chol in Gromacs format. The Supporting Information is available free of charge on the ACS Publications website at DOI: 10.1021/acs.jpcb.5b05522.

AUTHOR INFORMATION

Corresponding Author

*E-mail karel.berka@upol.cz. Phone: +420-58 563 4769.

Notes

The authors declare no competing financial interest.

ACKNOWLEDGMENTS

Thanks to Jeff Klauda for sharing CHARMM36 parameters of Cer ahead of publication. We gratefully acknowledge support through Project LO1305 of the Ministry of Education, Youth and Sports of the Czech Republic. M.O. acknowledges support from the Czech Grant Agency through Project P208/12/G016. M.P. acknowledges support from a student project of Palacký University Olomouc (IGA_Prf_2015_027). Ž.S. was supported by the Operational Program Education for Competitiveness European Social Fund (Projects CZ.1.07/2.3.00/30.0041). The access of Ž.S. to computing and storage facilities owned by parties and projects contributing to the National Grid Infrastructure MetaCentrum and IT4Innovations (LM2010005 and LM2011033) is greatly appreciated.

REFERENCES

- (1) Menon, G. K.; Cleary, G. W.; Lane, M. E. The Structure and Function of the Stratum Corneum. *Int. J. Pharm.* **2012**, *435*, 3–9.
- (2) Van Meer, G.; Voelker, D. R.; Feigenson, G. W. Membrane Lipids: Where They Are and How They Behave. *Nat. Rev. Mol. Cell Biol.* **2008**, *9*, 112–124.
- (3) Wertz, P. W. Lipids and Barrier Function of the Skin. *Acta Dermato-Venereologica, Suppl.* **2000**, *80*, 7–11.
- (4) Pascher, I. Molecular Arrangements in Sphingolipids. Conformation and Hydrogen Bonding of Ceramide and Their Implication on Membrane Stability and Permeability. *Biochim. Biophys. Acta, Biomembr.* **1976**, *455*, 433–451.
- (5) Guo, S.; Moore, T. C.; Iacobella, C. R.; Strickland, L. A.; McCabe, C. Simulation Study of the Structure and Phase Behavior of Ceramide Bilayers and the Role of Lipid Head Group Chemistry. *J. Chem. Theory Comput.* **2013**, *9*, 5116–5126.
- (6) Pascher, I.; Sundell, S. Molecular Arrangements in Sphingolipids: Crystal Structure of the Ceramide. *Chem. Phys. Lipids* **1992**, *62*, 79–86.
- (7) Sovová, Ž.; Berka, K.; Otyepka, M.; Jurečka, P. Coarse-Grain Simulations of Skin Ceramide NS with Newly Derived Parameters Clarify Structure of Melted Phase. *J. Phys. Chem. B* **2015**, *119*, 3988–3998.
- (8) Palonciová, M.; DeVane, R. H.; Murch, B. P.; Berka, K.; Otyepka, M. Rationalization of Reduced Penetration of Drugs through Ceramide Gel Phase Membrane. *Langmuir* **2014**, *30*, 13942–13948.
- (9) Wertz, P. W. Current Understanding of Skin Biology Pertinent to Skin Penetration: Skin Biochemistry. *Skin Pharmacol. Physiol.* **2013**, *26*, 217–226.
- (10) Elias, P. M.; Friend, D. S. The Permeability Barrier in Mammalian Epidermis. *J. Cell Biol.* **1975**, *65*, 180–191.
- (11) Bouwstra, J. A.; Ponec, M. The Skin Barrier in Healthy and Diseased State. *Biochim. Biophys. Acta, Biomembr.* **2006**, *1758*, 2080–2095.
- (12) Holleran, W. M.; Takagi, Y.; Uchida, Y. Epidermal Sphingolipids: Metabolism, Function, and Roles in Skin Disorders. *FEBS Lett.* **2006**, *580*, 5456–5466.
- (13) Janssens, M.; van Smeden, J.; Gooris, G. S.; Bras, W.; Portale, G.; Caspers, P. J.; Vreeken, R. J.; Hankemeier, T.; Kezic, S.; Wolterbeek, R.; et al. Increase in Short-Chain Ceramides Correlates with an Altered Lipid Organization and Decreased Barrier Function in Atopic Eczema Patients. *J. Lipid Res.* **2012**, *53*, 2755–2766.
- (14) Janssens, M.; van Smeden, J.; Gooris, G. S.; Bras, W.; Portale, G.; Caspers, P. J.; Vreeken, R. J.; Kezic, S.; Lavrijsen, A. P. M.; Bouwstra, J. A. Lamellar Lipid Organization and Ceramide Composition in the Stratum Corneum of Patients with Atopic Eczema. *J. Invest. Dermatol.* **2011**, *131*, 2136–2138.
- (15) Tawada, C.; Kanoh, H.; Nakamura, M.; Mizutani, Y.; Fujisawa, T.; Banno, Y.; Seishima, M. Interferon- γ Decreases Ceramides with Long-chain Fatty Acids: Possible Involvement in Atopic Dermatitis and Psoriasis. *J. Invest. Dermatol.* **2014**, *134*, 712–718.
- (16) Eckl, K.-M.; Tidhar, R.; Thiele, H.; Oji, V.; Haussler, I.; Brodesser, S.; Preil, M.-L.; Onal-Akan, A.; Stock, F.; Müller, D.; et al. Impaired Epidermal Ceramide Synthesis Causes Autosomal Recessive Congenital Ichthyosis and Reveals the Importance of Ceramide Acyl Chain Length. *J. Invest. Dermatol.* **2013**, *133*, 2202–2211.
- (17) Abraham, W.; Downing, D. T. Preparation of Model Membranes for Skin Permeability Studies Using Stratum Corneum Lipids. *J. Invest. Dermatol.* **1989**, *93*, 809–813.
- (18) Janušová, B.; Zbytovská, J.; Lorenc, P.; Vavrysová, H.; Palát, K.; Hrabálek, A.; Vávrová, K. Effect of Ceramide Acyl Chain Length on Skin Permeability and Thermotropic Phase Behavior of Model Stratum Corneum Lipid Membranes. *Biochim. Biophys. Acta, Mol. Cell Biol. Lipids* **2011**, *1811*, 129–137.
- (19) Školová, B.; Janušová, B.; Zbytovská, J.; Gooris, G.; Bouwstra, J.; Slepčík, P.; Berka, P.; Roh, J.; Palát, K.; Hrabálek, A.; et al. Ceramides in the Skin Lipid Membranes: Length Matters. *Langmuir* **2013**, *29*, 15624–15633.
- (20) Marrink, S.-J.; Berendsen, H. J. C. Simulation of Water Transport through a Lipid Membrane. *J. Phys. Chem.* **1994**, *98*, 4155–4168.
- (21) Orsi, M.; Essex, J. W. Permeability of Drugs and Hormones through a Lipid Bilayer: Insights from Dual-Resolution Molecular Dynamics. *Soft Matter* **2010**, *6*, 3797–3808.
- (22) Notman, R.; Anwar, J. Breaching the Skin Barrier - Insights from Molecular Simulation of Model Membranes. *Adv. Drug Delivery Rev.* **2013**, *65*, 237–250.
- (23) Höltje, M.; Förster, T.; Brandt, B.; Engels, T.; von Rybinski, W.; Höltje, H. D. Molecular Dynamics Simulations of Stratum Corneum Lipid Models: Fatty Acids and Cholesterol. *Biochim. Biophys. Acta, Biomembr.* **2001**, *1511*, 156–167.
- (24) Das, C.; Noro, M. G.; Olmsted, P. D. Simulation Studies of Stratum Corneum Lipid Mixtures. *Biophys. J.* **2009**, *97*, 1941–1951.
- (25) Torin Huzil, J.; Sivaloganathan, S.; Kohandel, M.; Foldvari, M. Drug Delivery through the Skin: Molecular Simulations of Barrier Lipids to Design More Effective Noninvasive Dermal and Transdermal Delivery Systems for Small Molecules, Biologics, and Cosmetics. *Wiley Interdiscip. Rev. Nanomed. Nanobiotechnol.* **2011**, *3*, 449–462.
- (26) Pandit, S. A.; Scott, H. L. Molecular-Dynamics Simulation of a Ceramide Bilayer. *J. Chem. Phys.* **2006**, *124*, 014708.
- (27) Hadley, K. R.; McCabe, C. A Simulation Study of the Self-Assembly of Coarse-Grained Skin Lipids. *Soft Matter* **2012**, *8*, 4802–4814.
- (28) MacDermaid, C. M.; DeVane, R. H.; Klein, M. L.; Fiorin, G. Dehydration of Multilamellar Fatty Acid Membranes: Towards a Computational Model of the Stratum Corneum. *J. Chem. Phys.* **2014**, *141*, 22D526.
- (29) Neale, C.; Bennett, W. F. D.; Tielemans, D. P.; Pomès, R. Statistical Convergence of Equilibrium Properties in Simulations of Molecular Solutes Embedded in Lipid Bilayers. *J. Chem. Theory Comput.* **2011**, *7*, 4175–4188.
- (30) Palonciová, M.; Berka, K.; Otyepka, M. Convergence of Free Energy Profile of Coumarin in Lipid Bilayer. *J. Chem. Theory Comput.* **2012**, *8*, 1200–1211.
- (31) Notman, R.; den Otter, W. K.; Noro, M. G.; Briels, W. J.; Anwar, J. The Permeability Enhancing Mechanism of DMSO in Ceramide Bilayers Simulated by Molecular Dynamics. *Biophys. J.* **2007**, *93*, 2056–2068.
- (32) Das, C.; Olmsted, P.; Noro, M. Water Permeation through Stratum Corneum Lipid Bilayers from Atomistic Simulations. *Soft Matter* **2009**, *5*, 4549–4556.
- (33) Notman, R.; Anwar, J.; Briels, W. J.; Noro, M. G.; den Otter, W. K. Simulations of Skin Barrier Function: Free Energies of Hydro-

- phobic and Hydrophilic Transmembrane Pores in Ceramide Bilayers. *Biophys. J.* **2008**, *95*, 4763–4771.
- (34) Klauda, J. B.; Venable, R. M.; Freites, J. A.; O'Connor, J. W.; Tobias, D. J.; Mondragon-Ramirez, C.; Vorobyov, I.; MacKerell, A. D.; Pastor, R. W.; Connor, J. W. O.; et al. Update of the CHARMM All-Atom Additive Force Field for Lipids: Validation on Six Lipid Types. *J. Phys. Chem. B* **2010**, *114*, 7830–7843.
- (35) Palonciová, M.; Fabre, G.; Devane, R. H.; Trouillas, P.; Berka, K.; Otyepka, M. Benchmarking of Force Fields for Molecule–Membrane Interactions. *J. Chem. Theory Comput.* **2014**, *10*, 4143–4151.
- (36) Venable, R. M.; Sodt, A. J.; Rogaski, B.; Rui, H.; Hatcher, E.; MacKerell, A. D.; Pastor, R. W.; Klauda, J. B. CHARMM All-Atom Additive Force Field for Sphingomyelin: Elucidation of Hydrogen Bonding and of Positive Curvature. *Biophys. J.* **2014**, *107*, 134–145.
- (37) Marrink, S. J.; Risselada, H. J.; Yefimov, S.; Tieleman, D. P.; de Vries, A. H. The MARTINI Force Field: Coarse Grained Model for Biomolecular Simulations. *J. Phys. Chem. B* **2007**, *111*, 7812–7824.
- (38) Pastor, R. W.; MacKerell, A. D. Development of the CHARMM Force Field for Lipids. *J. Phys. Chem. Lett.* **2011**, *2*, 1526–1532.
- (39) Vanommeslaeghe, K.; Hatcher, E.; Acharya, C.; Kundu, S.; Zhong, S.; Shim, J.; Darian, E. CHARMM General Force Field: A Force Field for Drug-Like Molecules Compatible with the CHARMM All-Atom Additive Biological Force Fields. *J. Comput. Chem.* **2009**, *31*, 671–690.
- (40) Van Der Spoel, D.; Lindahl, E.; Hess, B.; Groenhof, G.; Mark, A. E.; Berendsen, H. J. C. GROMACS: Fast, Flexible, and Free. *J. Comput. Chem.* **2005**, *26*, 1701–1718.
- (41) Hess, B.; Kutzner, C.; van der Spoel, D.; Lindahl, E. GROMACS 4: Algorithms for highly efficient, load-balanced, and scalable molecular simulation. *J. Chem. Theory Comput.* **2008**, *4*, 435–447.
- (42) Nose, S. A Unified Formulation of the Constant Temperature Molecular Dynamics Methods. *J. Chem. Phys.* **1984**, *81*, 511–519.
- (43) Hoover, W. G. Canonical Dynamics: Equilibrium Phase-Space Distributions. *Phys. Rev. A: At., Mol., Opt. Phys.* **1985**, *31*, 1695–1697.
- (44) Parrinello, M.; Rahman, A. Polymorphic Transitions in Single Crystals: A New Molecular Dynamics Method. *J. Appl. Phys.* **1981**, *52*, 7182–7190.
- (45) Xiang, T. X.; Anderson, B. D. Permeability of Acetic Acid across Gel and Liquid-crystalline Lipid Bilayers Conforms to Free-Surface-Area Theory. *Biophys. J.* **1997**, *72*, 223–237.
- (46) Bussi, G.; Donadio, D.; Parrinello, M. Canonical Sampling Through Velocity Rescaling. *J. Chem. Phys.* **2007**, *126*, 014101.
- (47) Berendsen, H.; Postma, J.; Vangunsteren, W.; Dinola, A.; Haak, J. Molecular-Dynamics with Coupling to an External Bath. *J. Chem. Phys.* **1984**, *81*, 3684–3690.
- (48) Pogor, D.; van Gunsteren, W. F.; Mark, A. E. A New Force Field for Simulating Phosphatidylcholine Bilayers. *J. Comput. Chem.* **2010**, *31*, 1117–1125.
- (49) Engelbrecht, T. N.; Schroeter, A.; Hauß, T.; Demé, B.; Scheidt, H. a.; Huster, D.; Neubert, R. H. H. The Impact of Ceramides NP and AP on the Nanostructure of Stratum Corneum Lipid Bilayer. Part I: Neutron Diffraction and ²H NMR Studies on Multilamellar Models Based on Ceramides with Symmetric Alkyl Chain Length Distribution. *Soft Matter* **2012**, *8*, 2599–2607.
- (50) Vaknin, D.; Kelley, M. S. The Structure of D-Erythro-C18 Ceramide at the Air-Water Interface. *Biophys. J.* **2000**, *79*, 2616–2623.
- (51) Leekumjorn, S.; Sum, A. K. Molecular Studies of the Gel to Liquid-Crystalline Phase Transition for Fully Hydrated DPPC and DPPE Bilayers. *Biochim. Biophys. Acta, Biomembr.* **2007**, *1768*, 354–365.
- (52) Krause, M. R.; Regen, S. L. The Structural Role of Cholesterol in Cell Membranes: From Condensed Bilayers to Lipid Rafts. *Acc. Chem. Res.* **2014**, *47*, 3512–3521.
- (53) Westerlund, B.; Grandell, P. M.; Isaksson, Y. J. E.; Slotte, J. P. Ceramide Acyl Chain Length Markedly Influences Miscibility with Palmitoyl Sphingomyelin in Bilayer Membranes. *Eur. Biophys. J.* **2010**, *39*, 1117–1128.
- (54) Ohvo-Rekilä, H.; Ramstedt, B.; Leppimäki, P.; Slotte, J. P. Cholesterol Interactions with Phospholipids in Membranes. *Prog. Lipid Res.* **2002**, *41*, 66–97.
- (55) Mitragotri, S. Modeling Skin Permeability to Hydrophilic and Hydrophobic Solutes Based on Four Permeation Pathways. *J. Controlled Release* **2003**, *86*, 69–92.
- (56) Vávrová, K.; Hrabálek, A.; Mac-Mary, S.; Humbert, P.; Muret, P. Ceramide Analogue 14S24 Selectively Recovers Perturbed Human Skin Barrier. *Br. J. Dermatol.* **2007**, *157*, 704–712.
- (57) Jurkiewicz, P.; Olzyńska, A.; Cwiklik, L.; Conte, E.; Jungwirth, P.; Megli, F. M.; Hof, M. Biophysics of Lipid Bilayers Containing Oxidatively Modified Phospholipids: Insights from Fluorescence and EPR Experiments and from MD Simulations. *Biochim. Biophys. Acta, Biomembr.* **2012**, *1818*, 2388–2402.
- (58) Johnson, M. E.; Blankschtein, D.; Langer, R. Evaluation of Solute Permeation through the Stratum Corneum: Lateral Bilayer Diffusion as the Primary Transport Mechanism. *J. Pharm. Sci.* **1997**, *86*, 1162–1172.
- (59) Norlén, L.; Gil, I. P.; Simonsen, A.; Descouts, P. Human Stratum Corneum Lipid Organization as Observed by Atomic Force Microscopy on Langmuir-Blodgett Films. *J. Struct. Biol.* **2007**, *158*, 386–400.
- (60) Kiselev, M. A.; Ryabova, N. Y.; Balagurov, A. M.; Dante, S.; Hauss, T.; Zbytovska, J.; Wartewig, S.; Neubert, R. H. H. New Insights into the Structure and Hydration of a Stratum Corneum Lipid Model Membrane by Neutron Diffraction. *Eur. Biophys. J.* **2005**, *34*, 1030–1040.